Commun Nonlinear Sci Numer Simulat 14 (2009) 4204–4219

Contents lists available at ScienceDirect

Commun Nonlinear Sci Numer Simulat

journal homepage: www.elsevier.com/locate/cnsns

Nonlinear dynamics of unicycles in leader–follower formation

Siming Zhao, Abhishek Halder, Tamás Kalmár-Nagy *

Department of Aerospace Engineering, Texas A&M University, College Station, TX 77843, USA

ARTICLE INFO

Article history:
Received 21 November 2008
Received in revised form 19 February 2009
Accepted 19 February 2009
Available online 13 March 2009

PACS:
05.45.−a
82.40.Bj

Keywords:
Unicycles
Formation stability
Hopf bifurcation
Nonlinear dynamics

ABSTRACT

In this paper, a dynamical systems analysis is presented for characterizing the motion of a group of unicycles in leader–follower formation. The equilibrium formations are characterized along with their local stability analysis. It is demonstrated that with the variation in control gain, the collective dynamics might undergo Andronov–Hopf and Fold–Hopf bifurcations. The vigor of quasi-periodicity in the regime of Andronov–Hopf bifurcation and heteroclinic bursts between quasi-periodic and chaotic behavior in the regime of Fold–Hopf bifurcation increases with the number of unicycles. Numerical simulations also suggest the occurrence of global bifurcations involving the destruction of heteroclinic orbit.

1. Introduction

Equilibrium formations for nonholonomic systems have been an active area of research in recent times among many disciplines like biological sciences [1–3], computer graphics [4] and systems engineering [5–8]. One particular problem studied in this context has been the *consensus seeking* [9] or the *state agreement problem* [10] which deals with designing feedback controllers to make multiple agents converge to a common configuration in the global coordinates. A special case to this is the *rendezvous problem* [11,12] where the agents converge at a single location.

In addition to the stability and control aspects, considerable efforts have also been put in effective modeling of the nonholonomic systems to make the analysis tractable. Starting from the *n*-bug problem in mathematics [13], the self-propelled planar particles were later [14,15] replaced by wheeled mobile agents with single nonholonomic constraint, i.e. unicycles. Lie group formulation [16] and oscillator models [17] have been attempted for dynamic modeling of such agents. In particular, Klein and Morgansen [18] extended the oscillator model to account for the intermediate centroid velocity of the unicycles to make trajectory tracking possible.

Several researchers [14,15,19–21] proposed laws for designing control strategies of such nonholonomic vehicles. One possible approach to design the control law is to use a centralized cooperative control scheme for the entire agent collective. However, such a control law is susceptible to bandwidth limitation as well as external disturbances and hence not scalable for a team having large number of mobile agents. As a result, distributed control laws have been investigated by the researchers for this problem, where the feedback is constructed through local interactions of the vehicles leading to a global formation convergence. In particular, Yang et al. [22,23] proposed a decentralized framework where a distributed controller accounts for local control decision based on the interaction of each agent with its neighbors.

* Corresponding author.
E-mail address: cnsns@kalmarnagy.com (T. Kalmár-Nagy).

1007-5704/$ - see front matter © 2009 Elsevier B.V. All rights reserved.
doi:10.1016/j.cnsns.2009.02.028

Moreover, their algorithm was also capable of estimating the global statistics of the swarm (for example, overall swarm shape), thereby enabling simultaneous estimation and control. A special research topic has been to design the distributed controller with asynchronous communication constraints. For a detailed account on this topic, the reader may refer [24–27].

The present paper is part of a research endeavor which aims to address the nonholonomic multi-agent dynamics and distributed control problem. The authors earlier studied [28] the cyclic pursuit of 2-unicycle problem with a controller similar to [14] in modified form. These preliminary results showed that the system may exhibit very different dynamics depending on the choice of controller gains. As a next step, in this paper, the authors study nonlinear dynamics of multiple nonholonomic unicycles in leader–follower configuration to characterize regimes of linear stability. Nonlinear analysis is also performed, which throws light in many nontrivial areas of the complex dynamics of the agents leading to greater understanding of the overall system.

The differences in the recent research directions in multi-agent systems has generally varied with the variety of control strategies and the types of consensus demanded. To the best of the authors' knowledge, very few attempts (like [29]) have been made to understand the system from the standpoint of nonlinear dynamics. The authors must underline the fact that a successful analysis to even slightly simpler systems like leader–follower configuration, can guide us in better designing of controllers.

As mentioned above, the choice of leader–follower configuration was partly due to its slightly simpler dynamics and partly due to the fact that many biological systems (like birds) also exhibit this configuration. This choice, in the biological world was long believed to be for energy efficiency [30]. Some recent results [31] tell that leader–follower configuration may also enhance communication and orientation of the flock. It is a topic of research whether this form may have any superiority in inter-agent communication and performance for the bio-mimetic collectives.

The rest of this paper is organized as follows. Section 2 describes the mathematical model of the leader–follower formation and transforms the equations of motion from global to relative coordinates. Section 3 provides the derivation of fixed points followed by corresponding equilibrium formations. Section 4 presents the stability boundary based on local stability analysis and associated Hurwitz stability criteria. Section 5 presents the existence of Andronov–Hopf bifurcation depending on the value of scaled control gain followed by numerical simulation results presented in Section 6. Section 7 concludes the paper.

2. Mathematical model

The focus of this paper is to investigate the dynamics of an n-unicycle system with kinematic equations given by

$$\begin{pmatrix} \dot{x}_j(t) \\ \dot{y}_j(t) \\ \dot{\theta}_j(t) \end{pmatrix} = \begin{pmatrix} \cos\theta_j(t) & 0 \\ \sin\theta_j(t) & 0 \\ 0 & 1 \end{pmatrix} \begin{pmatrix} \upsilon_j \\ \omega_j \end{pmatrix}, \quad j = 0, 1, \ldots, n-1, \tag{1}$$

where the position and orientation of the jth vehicle are denoted by $x_j, y_j \in \mathbb{R}$ and $\theta_j \in [-\pi, \pi)$, respectively. υ_j and ω_j are the control inputs (linear velocity and angular velocity). The vehicle with index 0 will be referred to as the *leader*, and the others as *followers*. Our focus here is to analyze the leader–follower formation, when the trajectory of the leader is a straight line or a circle. These trajectories for the leader are obtained by the simple control law

$$\begin{aligned} \upsilon_0 &= V, \\ \omega_0 &= \omega. \end{aligned} \tag{2}$$

The case $\omega = 0$ represents straight line motion, while $\omega \neq 0$ corresponds to circular motion.

The configuration of the n-unicycle system is shown in Fig. 1, where r_i is the relative distance between the two vehicles, α_i is the angle between the current orientation of the ith unicycle and the line of sight, and β_i is the angle between the current orientation of $i+1$th unicycle and the line of sight. Both angles are positive in the sense of counterclockwise rotation to the line of sight. Following [14], the kinematic equations are written in relative coordinates:

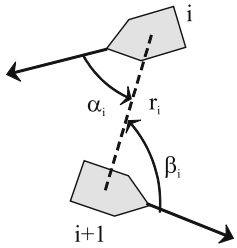

Fig. 1. Relative coordinates with vehicle $i+1$ pursuing vehicle i.

$$\begin{cases} \dot{r}_0 = -v_0 \cos\alpha_0 - v_1 \cos\beta_0, \\ \dot{\alpha}_0 = \frac{1}{r_0}(v_0 \sin\alpha_0 + v_1 \sin\beta_0) - \omega_0, \\ \dot{\beta}_0 = \frac{1}{r_0}(v_0 \sin\alpha_0 + v_1 \sin\beta_0) - \omega_1, \end{cases}$$
$$\begin{cases} \dot{r}_i = -v_i \cos\alpha_i - v_{i+1} \cos\beta_i, \\ \dot{\alpha}_i = \frac{1}{r_i}(v_i \sin\alpha_i + v_{i+1} \sin\beta_i) - \omega_i, \\ \dot{\beta}_i = \frac{1}{r_i}(v_i \sin\alpha_i + v_{i+1} \sin\beta_i) - \omega_{i+1}, \end{cases} \tag{3}$$

where $i = 1, \ldots, n-2$, $r_i \in \mathbb{R}^+$ and $(\alpha_i, \beta_i) \in \mathscr{S}^1 \times \mathscr{S}^1$. The pursuit control law for the ith follower is chosen as

$$\begin{aligned} v_i &= r_{i-1}, \\ \omega_i &= k \sin\beta_{i-1}, \end{aligned} \tag{4}$$

where the gain k is positive. The choice of this control law is inspired by the goal to align the follower's instantaneous velocity vector with its line of sight.

Substituting the control laws (2) and (4) into the relative dynamics (3) yields $n-1$ sets of three dimensional ODEs:

$$\begin{cases} \dot{r}_0 = -V \cos\alpha_0 - r_0 \cos\beta_0, \\ \dot{\alpha}_0 = \frac{1}{r_0}(V \sin\alpha_0 + r_0 \sin\beta_0) - \omega, \\ \dot{\beta}_0 = \frac{1}{r_0}(V \sin\alpha_0 + r_0 \sin\beta_0) - k \sin\beta_0, \end{cases}$$
$$\begin{cases} \dot{r}_i = -r_{i-1} \cos\alpha_i - r_i \cos\beta_i, \\ \dot{\alpha}_i = \frac{1}{r_i}(r_{i-1} \sin\alpha_i + r_i \sin\beta_i) - k \sin\beta_{i-1}, \\ \dot{\beta}_i = \frac{1}{r_i}(r_{i-1} \sin\alpha_i + r_i \sin\beta_i) - k \sin\beta_i, \end{cases} \tag{5}$$

The parameters of this system are V, ω and k and are restricted to be positive without loss of generality.

3. Characterization of equilibria

3.1. Derivation of the fixed points

Setting the right-hand side of (5) to zero results $3n-3$ transcendental equations for the fixed points of the system

$$\frac{V}{r_0^*} \cos\alpha_0^* = -\cos\beta_0^*, \tag{6}$$
$$\frac{V}{r_0^*} \sin\alpha_0^* = -\sin\beta_0^* + \omega, \tag{7}$$
$$\frac{V}{r_0^*} \sin\alpha_0^* = (k-1)\sin\beta_0^*, \tag{8}$$
$$\frac{r_{i-1}^*}{r_i^*} \cos\alpha_i^* = -\cos\beta_i^*, \tag{9}$$
$$\frac{r_{i-1}^*}{r_i^*} \sin\alpha_i^* = -\sin\beta_i^* + k \sin\beta_{i-1}^*, \tag{10}$$
$$\frac{r_{i-1}^*}{r_i^*} \sin\alpha_i^* = (k-1)\sin\beta_i^*. \tag{11}$$

Subtracting (7) from (8) and (10) from (11) yields

$$\sin\beta_0^* = \sin\beta_1^* = \cdots = \sin\beta_{n-2}^* = \frac{\omega}{k}. \tag{12}$$

Fixed point(s) exist when $|\sin\beta^*| \leqslant 1$, i.e. $k \geqslant \omega$. When $k = \omega$, fixed points coalesce in a saddle-node bifurcation.

Squaring and adding (6) and (7), (9) and (10) yields

$$\left(\frac{V}{r_0^*}\right)^2 = \left(\frac{r_{i-1}^*}{r_i^*}\right)^2 = 1 + \omega^2 - \frac{2\omega^2}{k},$$

which results the equilibrium relative distance as

$$r_0^* = \frac{V}{\sqrt{1+\omega^2-\frac{2\omega^2}{k}}}, \quad r_i^* = \frac{V}{(1+\omega^2-\frac{2\omega^2}{k})^{\frac{i+1}{2}}}, \qquad 1+\omega^2-\frac{2\omega^2}{k} > 0, \ \ i = 1,2,\ldots,n-2. \tag{13}$$

Further, substituting (12) and (13) into (7) and (10) yields

$$\sin\alpha_0^* = \sin\alpha_1^* = \cdots = \sin\alpha_{n-2}^* = \frac{\omega - \frac{\omega}{k}}{\sqrt{1+\omega^2-\frac{2\omega^2}{k}}}. \tag{14}$$

From (6) and (9), it can be noted that $\cos\alpha_i^*$ and $\cos\beta_i^*$ must have different signs.

When $k > \omega$, every α_i^* can assume two distinct values in $[0, 2\pi]$ and thus there are 2^{n-1} possible fixed points of system (5). However, $2^{n-1}-2$ of these fixed points are spurious, as the geometric constraint of the equilibrium formation demands all unicycles to perform unidirectional translation in case of straight line formation and unidirectional rotation in case of cyclic formation. This constraint makes only the following two fixed points (A and B) possible:

$$A\begin{cases} r_0^* = \frac{V}{\sqrt{1+\omega^2-\frac{2\omega^2}{k}}}, \quad r_i^* = \frac{V}{(1+\omega^2-\frac{2\omega^2}{k})^{\frac{i+1}{2}}}, \\ \alpha_0^* = \alpha_1^* = \cdots = \alpha_{n-2}^* = \pi - \arcsin\omega\frac{k-1}{k\sqrt{1+\omega^2-\frac{2\omega^2}{k}}}, \\ \beta_0^* = \beta_1^* = \cdots = \beta_{n-2}^* = \arcsin\frac{\omega}{k}, \end{cases}$$

$$B\begin{cases} r_0^* = \frac{V}{\sqrt{1+\omega^2-\frac{2\omega^2}{k}}}, \quad r_i^* = \frac{V}{(1+\omega^2-\frac{2\omega^2}{k})^{\frac{i+1}{2}}}, \\ \alpha_0^* = \alpha_1^* = \cdots = \alpha_{n-2}^* = \arcsin\omega\frac{k-1}{k\sqrt{1+\omega^2-\frac{2\omega^2}{k}}}, \\ \beta_0^* = \beta_1^* = \cdots = \beta_{n-2}^* = \pi - \arcsin\frac{\omega}{k}. \end{cases}$$

When $k = \omega$, the two fixed points A and B coalesce in a saddle-node bifurcation.

3.2. Equilibrium formations

Fixed points A and B correspond to equilibrium formations of the leader–follower system in global coordinates (x, y, θ). The goal of this section is to characterize these formations. When $\omega = 0$, the trajectory of the leader can be expressed explicitly as

$$\begin{aligned} x_0(t) &= (V\cos\theta_0)t + x_0(0), \\ y_0(t) &= (V\sin\theta_0)t + y_0(0), \\ \theta_0(t) &= \theta_0(0), \end{aligned} \tag{15}$$

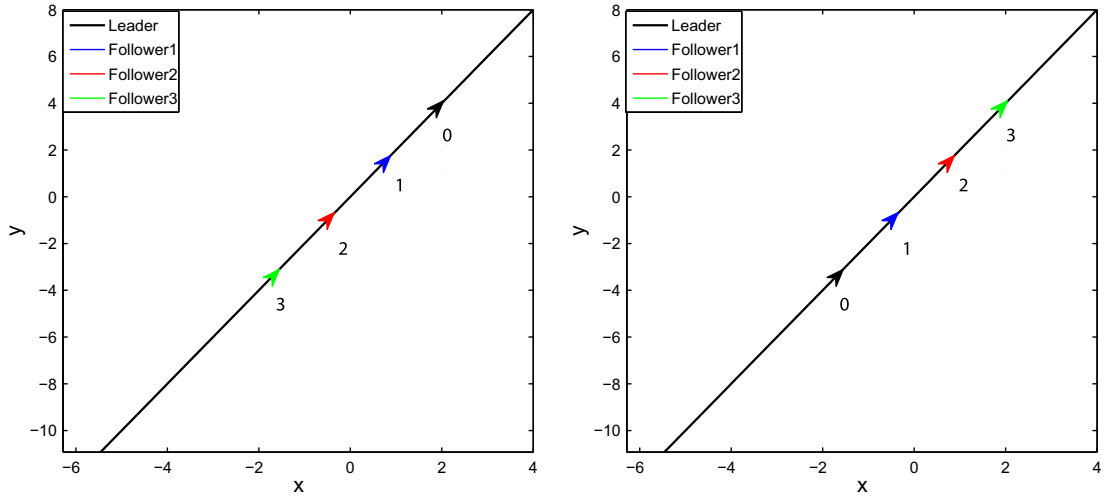

(a) Equilibrium formation for fixed point A (b) Equilibrium formation for fixed point B

Fig. 2. Corresponding straight-line motion in global coordinates for fixed points A and B.

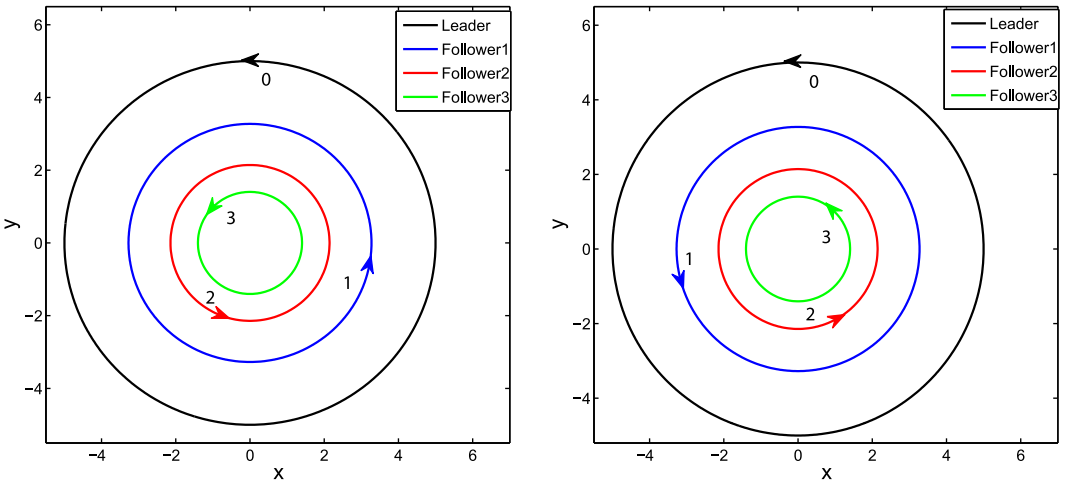

(a) Equilibrium formation for fixed point A (b) Equilibrium formation for fixed point B

Fig. 3. Corresponding circular motion in global coordinates for fixed points *A* and *B*.

where $x_0(0)$, $y_0(0)$, $\theta_0(0)$ are its initial positions and orientation. It is straightforward to observe that fixed points $A = (r_i^*, \alpha_i^*, \beta_i^*) = (V, \pi, 0)$ and $B = (r_i^*, \alpha_i^*, \beta_i^*) = (V, 0, \pi)$ correspond to rectilinear motion of the followers. Fig. 2 shows the corresponding "pursuit graph" (parametric plots of $\{x_i(t), y_i(t)\}$). It can be noted that for fixed point *A*, the leader "leads the pack" and for fixed point *B*, it trails it.

When $\omega \neq 0$, the trajectory of the leader becomes

$$x_0(t) = \frac{V}{\omega}\sin(\omega t + \theta) + x_c,$$
$$y_0(t) = -\frac{V}{\omega}\cos(\omega t + \theta) + y_c, \tag{16}$$
$$\theta_0(t) = \omega t + \theta_0(0), \tag{17}$$

where $x_c = x_0(0) - (V/\omega)\sin\theta_0(0)$ and $y_c = y_0(0) + (V/\omega)\cos\theta_0(0)$ are the center of the circle of radius $R_0 = (V/\omega)$ traversed by the leader. Without loss of generality we choose $x_c = y_c = 0$.

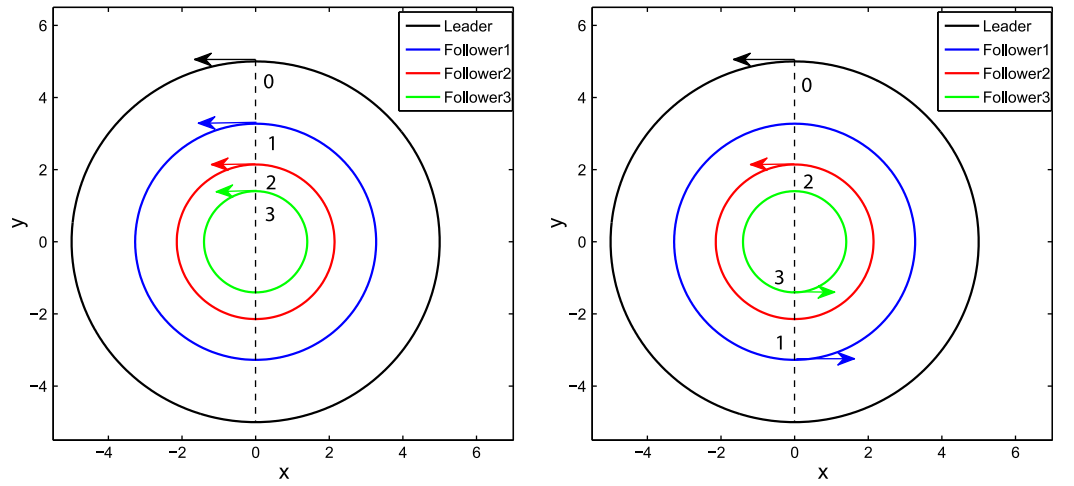

(a) Equilibrium formation when $k = \omega > 1$ (b) Equilibrium formation when $k = \omega < 1$

Fig. 4. Circular motion in global coordinates corresponding to the nonhyperbolic fixed point.

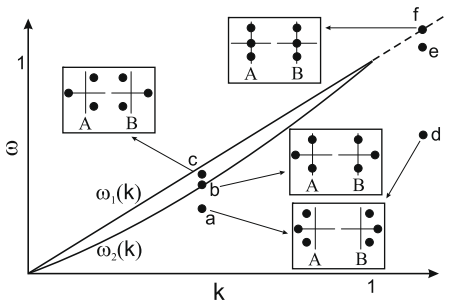

Fig. 5. Linear stability boundary for system (5) with spectra of A and B.

Both fixed points A and B yield the following two equations for the locus of the ith follower:

$$r_i^{*2} = \frac{V^2}{(1+\omega^2-\frac{2\omega^2}{k})^i} = x_i^2 + y_i^2 + x_{i+1}^2 + y_{i+1}^2 - 2(x_i x_{i+1} + y_i y_{i+1}), \tag{18}$$

$$\sin\alpha_i^* = \frac{\omega - \frac{\omega}{k}}{\sqrt{1+\omega^2-\frac{2\omega^2}{k}}} = \sin\arctan\left(\frac{y_{i+1}-y_i}{x_{i+1}-x_i} - \theta_i\right) = \frac{x_i^2 + y_i^2 - x_i x_{i+1} - y_i y_{i+1}}{r_i^*\sqrt{x_{i+1}^2 + y_{i+1}^2}}. \tag{19}$$

Since $x_0^2 + y_0^2 = (V^2/\omega^2)$ corresponds to the leader's $(j=0)$ trajectory, combining (18) and (19) results

$$x_1^2 + y_1^2 = \frac{V^2}{\omega^2}\frac{1}{1+\omega^2-\frac{2\omega^2}{k}} = R_1^2. \tag{20}$$

In general, using method of induction

$$x_j^2 + y_j^2 = \frac{V^2}{\omega^2}\frac{1}{(1+\omega^2-\frac{2\omega^2}{k})^j} = R_j^2. \tag{21}$$

This means that in the equilibrium formation, the jth follower is circling the origin with radius R_j. Fig. 3 shows the corresponding "pursuit graph" for fixed A and fixed point B for circular motion $(\omega > 0)$.

It can be noted from (21) that depending on the value of k, the concentric circles traced out by the followers can be inside $(k > 2)$, on $(k = 2)$ or outside $(k < 2)$ the leader's circle. Also, analogous to Fig. 2, for $k > 2$ case, corresponding to fixed point A, the leader "leads the pack", i.e. the followers have positive phase difference with respect to the leader (Fig. 3a). Similarly, for fixed point B, the leader "trails the pack", i.e. the followers have negative phase difference with respect to the leader (Fig. 3b).

As discussed in the previous section, the two fixed points A and B coalesce to give rise to the single nonhyperbolic fixed point $(r_i^*, \alpha_i^*, \beta_i^*) = (\frac{V}{(\omega-1)^{i+1}}, \frac{\pi}{2}, \frac{\pi}{2})$ $(k = \omega > 1)$ or $(r_i^*, \alpha_i^*, \beta_i^*) = \left(\frac{V}{(1-\omega)^{i+1}}, -\frac{\pi}{2}, \frac{\pi}{2}\right)$ (when $k = \omega < 1$). The two cases are illustrated in Fig. 4a and 4b

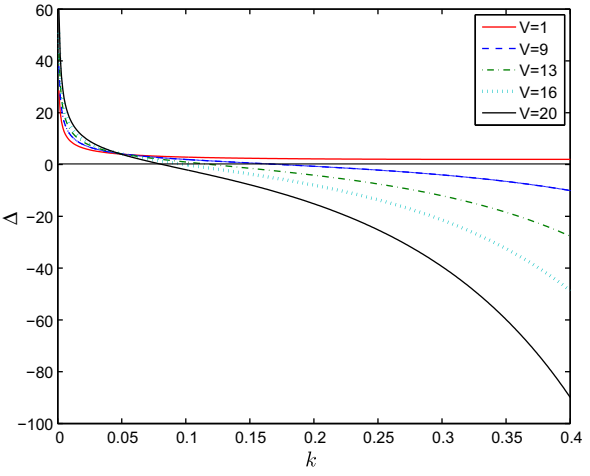

Fig. 6. Variation of Poincaré–Lyapunov constant (Δ) with control gain (k).

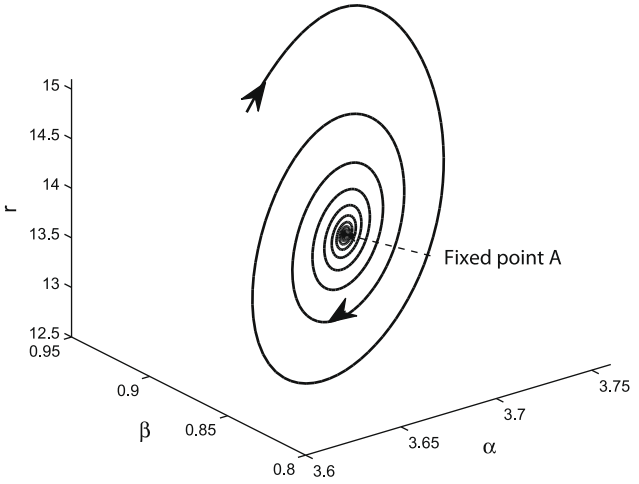

(a) Phase portrait at point a

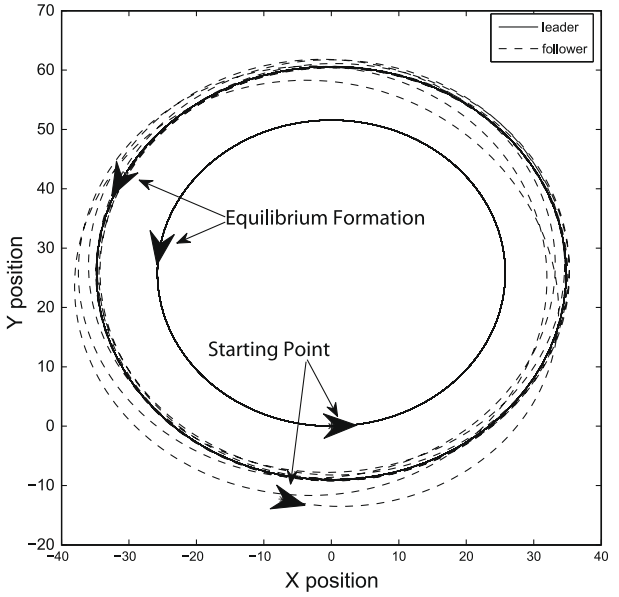

(b) Pursuit graph for point a in global coordinates

Fig. 7. Phase portrait at point a when fixed point *A* is attracting and the corresponding pursuit graph in global coordinates.

4. Local stability analysis

4.1. Linearization about the fixed points

The local stability of the fixed points is determined by the eigenstructure of the Jacobian evaluated at the fixed point. The Jacobian of (5) is given by

$$\mathscr{J}_p = \begin{pmatrix} \mathbf{A_0} & \mathbf{0} & \cdots & \mathbf{0} \\ \mathbf{B_1} & \mathbf{A}_1 & \cdots & \mathbf{0} \\ \vdots & \ddots & \ddots & \vdots \\ \mathbf{0} & \cdots & \mathbf{B_{n-2}} & \mathbf{A_{n-2}} \end{pmatrix}, \tag{22}$$

where $\mathbf{A_i}$, $\mathbf{B_i}$ and $\mathbf{0}$ are all 3×3 matrices.

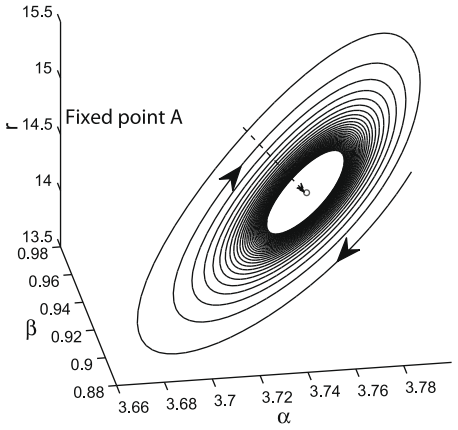

Fig. 8. Phase portrait at point b where the fixed point *A* is a weakly attracting one.

$$\mathbf{A}_0 = \begin{pmatrix} -\cos\beta_0^* & V\sin\alpha_0^* & r_0^*\sin\beta_0^* \\ -\frac{V}{r_0^{*2}}\sin\alpha_0^* & \frac{V}{r_0^*}\cos\alpha_0^* & \cos\beta_0^* \\ -\frac{V}{r_0^{*2}}\sin\alpha_0^* & \frac{V}{r_0^*}\cos\alpha_0^* & (1-k)\cos\beta_0^* \end{pmatrix},$$

$$\mathbf{A_i} = \begin{pmatrix} -\cos\beta_i^* & r_{i-1}^*\sin\alpha_i^* & r_i^*\sin\beta_i^* \\ -\frac{r_{i-1}^*}{r_i^{*2}}\sin\alpha_i^* & \frac{r_{i-1}^*}{r_i^*}\cos\alpha_i^* & \cos\beta_i^* \\ -\frac{r_{i-1}^*}{r_i^{*2}}\sin\alpha_i^* & \frac{r_{i-1}^*}{r_i^*}\cos\alpha_i^* & (1-k)\cos\beta_i^* \end{pmatrix}, \quad i = 1,2,\ldots,n-2,$$

$$\mathbf{B_i} = \begin{pmatrix} -\cos\alpha_i^* & 0 & 0 \\ \frac{\sin\alpha_i^*}{r_i^*} & 0 & -k\cos\beta_{i-1}^* \\ \frac{\sin\alpha_i^*}{r_i^*} & 0 & 0 \end{pmatrix}, \quad i = 1,2,\ldots,n-2.$$

The eigenvalues of (22) are also the eigenvalues of all $\mathbf{A_i}$'s since the Jacobian (22) is lower triangular block matrix. The characteristic polynomial for any of the $\mathbf{A_i}$'s evaluated at the fixed points have the same form and are given by (+ and − corresponds to fixed point *A* and *B*, resp.):

$$\lambda^3 \pm p_2\lambda^2 + p_1\lambda \pm p_0 = 0, \tag{23}$$

where $p_2 = (1+(1/k))\sqrt{k^2-\omega^2}$, $p_1 = \omega^2 + 2k - (3\omega^2/k)$ and $p_0 = (1+\omega^2-(2\omega^2/k))\sqrt{k^2-\omega^2}$. The characteristic equation corresponding to fixed point *B* can be obtained from that of fixed point *A* by the transformation $\lambda \to -\lambda$, so the spectrum of *B* is the reflection of that of *A* about the imaginary axis.

4.2. Linear stability boundary

A fixed point is stable when the corresponding characteristic polynomial is Hurwitz. Necessary and sufficient condition on Hurwitz stability of a third-order polynomial is given on p. 132 of [32], requiring $p_0, p_1, p_2 > 0$ and $p_1p_2 > p_0$ for (23), which results

$$2k^3 + k^2 - 3\omega^2 > 0, \tag{24}$$

$$1 + \omega^2 - \frac{2\omega^2}{k} > 0. \tag{25}$$

From (12), the existence of the fixed points requires

$$k \geqslant \omega. \tag{26}$$

Inequalities (24)–(26) determine regions in the k–ω parameter space where fixed points exists, as well as their stability. These regions are characterized by the three curves $\omega_1(k) = k$, $\omega_2(k) = \sqrt{\frac{2k^3+k^2}{3}}$ and $\omega_3(k) = \sqrt{\frac{k}{2-k}}$ $(k < 2)$. Notice that when $k \geqslant 2$, inequality (25) is alway satisfied, the stability region is determined only by the remaining two curves. It can be easily verified that $\omega_1(k) \leqslant \omega_3(k)$ when $0 < k < 2$. Fig. 5 depicts the stability boundaries of this system. It can be observed that when $\omega = 0$ (straight line motion), fixed point *A* is always a stable node, while *B* is always an unstable one.

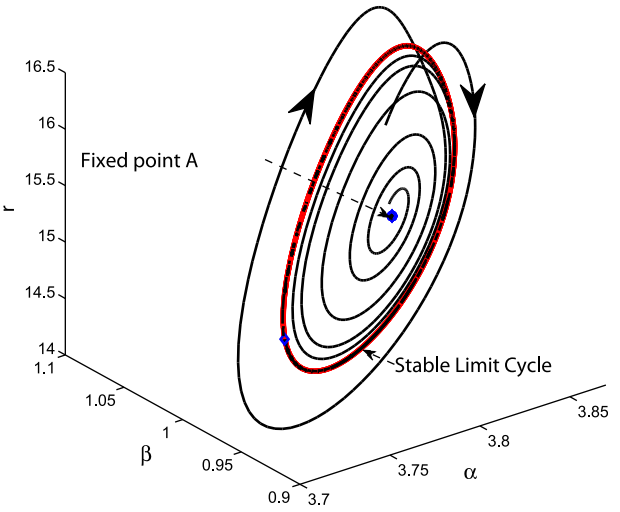

(a) Phase portrait at point c

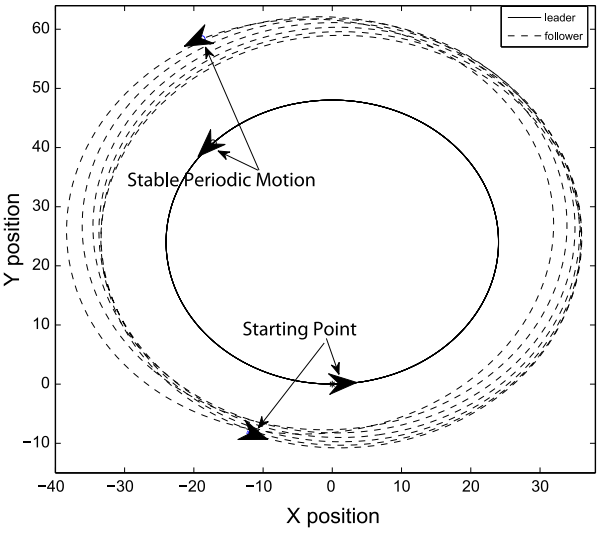

(b) Pursuit graph in global coordinates

Fig. 9. Phase portrait at point c $(k = 0.500,\ \omega = 0.409)$ when a stable limit cycle is born near fixed point A and the corresponding pursuit graph.

5. Andronov–Hopf bifurcation

When $0 < k < 1$, the characteristic polynomial on the curve $\omega_2(k)$ can be written as

$$\left(\lambda + \left(1 + \frac{1}{k}\right)\sqrt{k^2 - \omega^2}\right)\left(\lambda^2 + \omega^2 + 2k - \frac{3\omega^2}{k}\right) = 0.$$

This implies that for the fixed point A, the Jacobian has one negative real eigenvalue and a complex conjugate pair on the imaginary axis. Below the curve $\omega_2(k)$, the Jacobian has one negative real eigenvalue and a pair of complex conjugates on the left half plane, i.e. the fixed point is a stable node-focus. Between the curve $\omega_2(k)$ and $\omega_1(k)$, the pair of complex conjugate eigenvalues have positive real part, which suggests the occurrence of Andronov–Hopf bifurcation by increasing k through $\omega_2(k)$. On this curve, the critical bifurcation value of ω is $\omega_c = \sqrt{\frac{2k^3+k^2}{3}}$, and the root crossing velocity can be calculated as

$$\mathrm{Re}\left.\frac{d\lambda}{d\omega}\right|_{(k,\omega_c)} = \frac{3\sqrt{2}}{7k+2}\sqrt{\frac{1+2k}{1-k}} > 0. \tag{27}$$

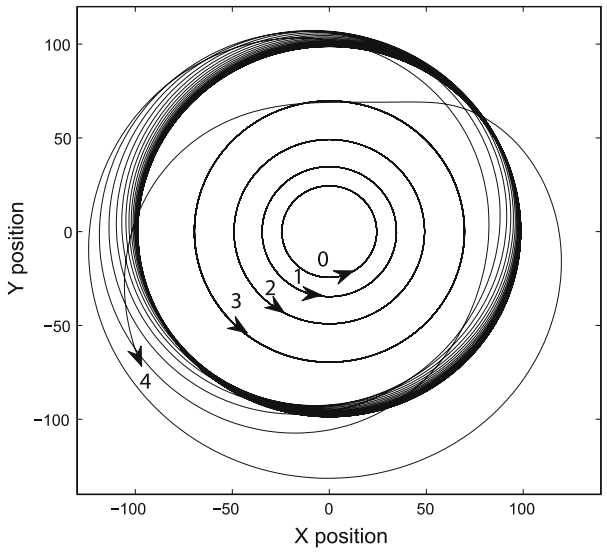

(a) Pursuit graph for five unicycles

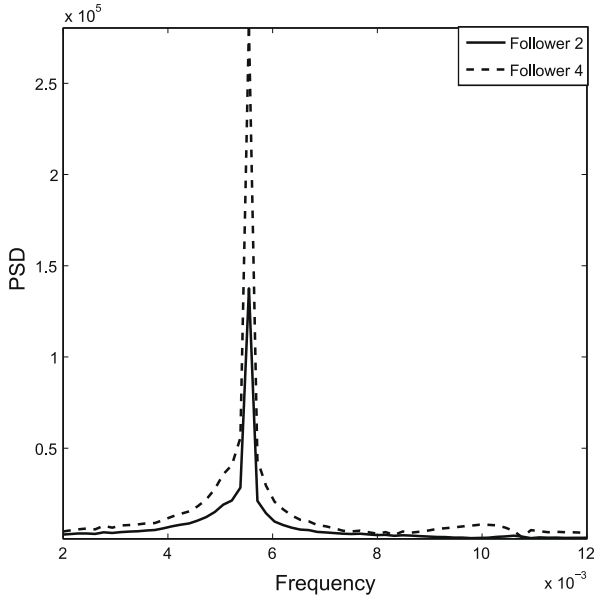

(b) Corresponding FFT of x_2 and x_4

Fig. 10. Pursuit graph and the corresponding FFT for five unicycle case at point *c*.

Transversal root crossing is a necessary condition for the Andronov–Hopf bifurcation. It can be noted that for the case of n unicycles, we have $n-1$ identical triplets of such eigenvalues. This implies that the system undergoes Andronov–Hopf bifurcation when $n=2$, double-Hopf bifurcation when $n=3$ and in general, a bifurcation with $(n-1)$ pairs of pure imaginary eigenvalues. The rest of this section analyzes the two unicycle case in detail.

To show that the fixed point of the dynamical system (5) is weakly attracting/repelling on the stability boundary, one needs to compute the so-called Poincaré–Lyapunov constant [33]. To find this constant, the original equation (5) is expanded up to third order around fixed point A [34]

$$\dot{\mathbf{w}} = \Psi(\mathbf{w}) = \mathscr{J}_p\mathbf{w} + \frac{1}{2}\mathbf{f}^{(2)}(\mathbf{w}) + \frac{1}{6}\mathbf{f}^{(3)}(\mathbf{w}) + \mathscr{O}(\mathbf{w}^4), \tag{28}$$

where $\mathbf{w} = (r - r_A^*, \alpha - \alpha_A^*, \beta - \beta_A^*)^T$ defines new coordinates which shift the fixed point A to the origin. In these new coordinates, $\mathbf{f}^{(2)}(\mathbf{w})$ and $\mathbf{f}^{(3)}(\mathbf{w})$ are multilinear vector functions given by

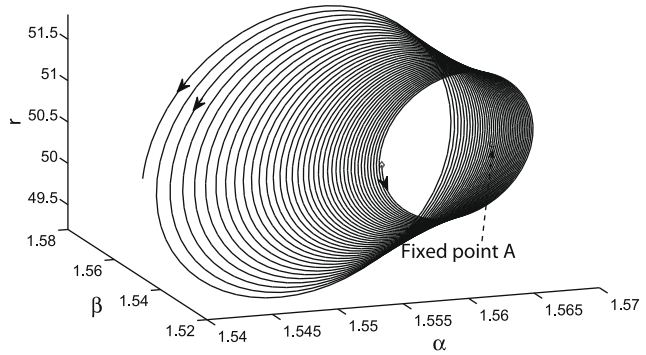

(a) Phase portrait at point f

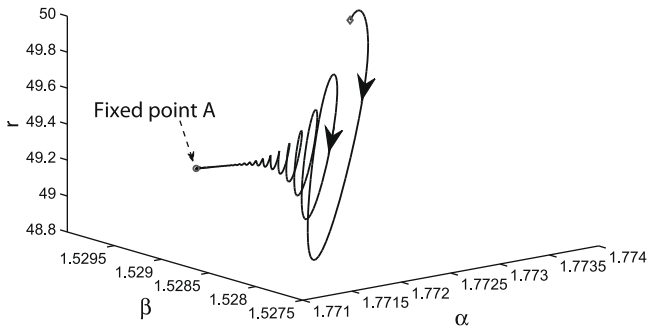

(b) Phase portrait at point e

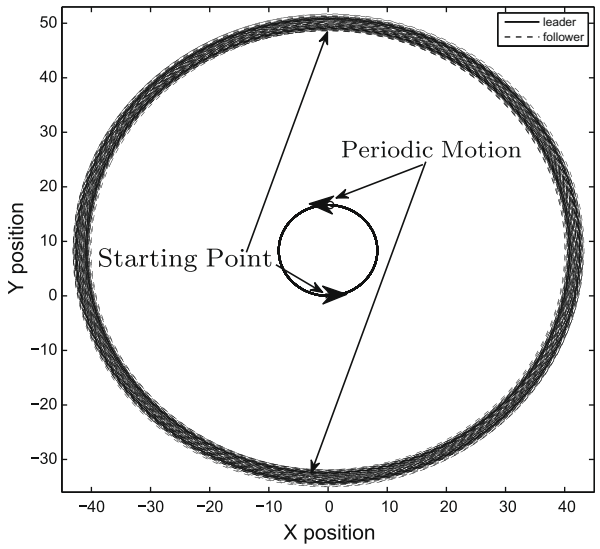

(c) Pursuit graph in global coordinates

Fig. 11. Phase portrait at point *f* near the fixed point *A* and the corresponding pursuit graph in global coordinates.

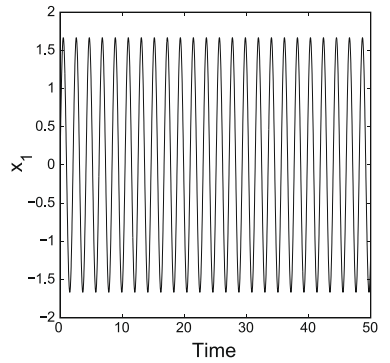

(a) Time series of x position of follower 1

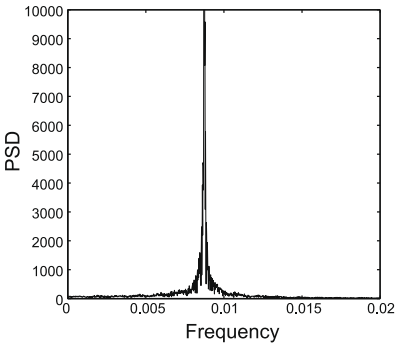

(b) FFT of x_1

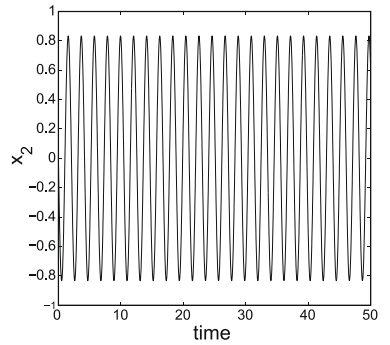

(c) Time series of x position of follower 2

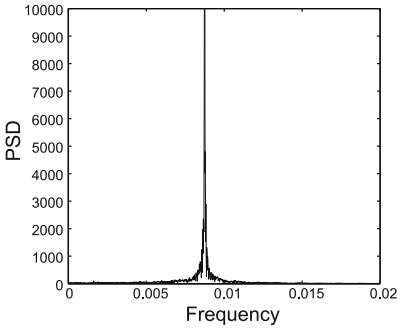

(d) FFT of x_2

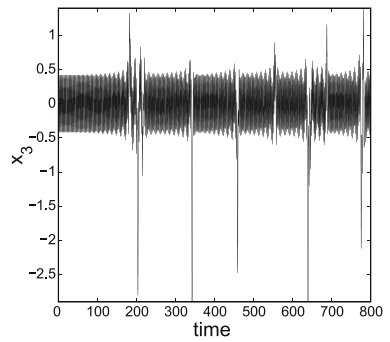

(e) Time series of x position of follower 3

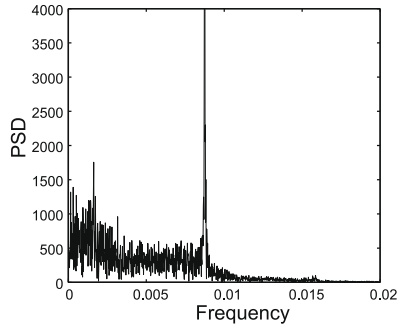

(f) FFT of x_3

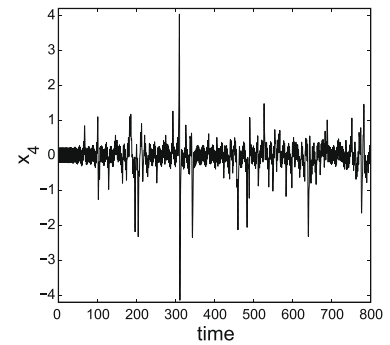

(g) Time series of x position of follower 4

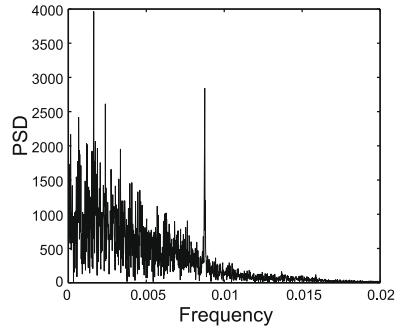

(h) FFT of x_4

Fig. 12. Time series and corresponding FFT for five unicycle case at point *f*.

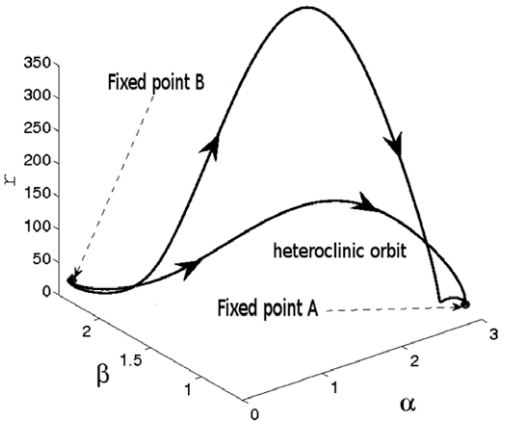

Fig. 13. Heteroclinic orbit in the phase portrait at point *d*.

$$\mathbf{f}_i^{(2)} = \sum_{j,k=1}^{n} \left.\frac{\partial^2 \boldsymbol{\Psi}_i(\xi)}{\partial\xi_j \partial\xi_k}\right|_{\xi=0} \mathbf{w}_j \mathbf{w}_k, \quad i = 1,2,3$$

and

$$\mathbf{f}_i^{(3)} = \sum_{j,k,l=1}^{n} \left.\frac{\partial^3 \boldsymbol{\Psi}_i(\xi)}{\partial\xi_j \partial\xi_k \partial\xi_l}\right|_{\xi=0} \mathbf{w}_j \mathbf{w}_k \mathbf{w}_l, \quad i = 1,2,3.$$

In order to obtain the real Jordan canonical form, a linear transformation $\mathbf{T}$ needs to be constructed using the eigenvectors of the Jacobian evaluated at ω_c. At the critical point, the pair of complex conjugate eigenvalues have the form $\lambda_{2,3} = \pm i\omega_0$,

$$\omega_0 = \sqrt{k\left(1 - \frac{2}{3}k\right)(1-k)} > 0.$$

Let $\mathbf{q}_2 \in \mathscr{C}^3$ be the complex eigenvector corresponding to the eigenvalue λ_2. Then,

$$\mathscr{J}_p \mathbf{q}_2 = i\omega_0 \mathbf{q}_2, \quad \mathscr{J}_p \bar{\mathbf{q}}_2 = -i\omega_0 \bar{\mathbf{q}}_2.$$

Also, let $\mathbf{q}_1 \in \mathscr{R}^3$ be the real eigenvector corresponding to the eigenvalue $\lambda_1 = -(1+k)\sqrt{\frac{2}{3}(1-k)}$, i.e. $\mathscr{J}_p \mathbf{q}_1 = \lambda_1 \mathbf{q}_1$. The transformation matrix $\mathbf{T}$ is composed by $\frac{1}{\|\mathbf{q}_1\|}(\mathrm{Re}\,\mathbf{q}_2, -\mathrm{Im}\,\mathbf{q}_2, \|\mathbf{q}_1\|\mathbf{q}_1)$ where $\mathbf{q}_1$ and $\mathbf{q}_2$ are given by

$$\mathbf{q}_2 = \begin{pmatrix} \frac{2\sqrt{6}Vk}{9\gamma\sqrt{1-k}} + i\frac{Vk(1-\frac{2}{3}k)}{3\omega_0\gamma} \\ 1 \\ 1 - \frac{2}{3}k + i\frac{\sqrt{6}\omega_0}{3\sqrt{1-k}} \end{pmatrix}, \quad \mathbf{q}_1 = \begin{pmatrix} -\frac{\sqrt{6}V(1+2k)}{3\gamma\sqrt{1-k}} \\ 1 \\ k+1 \end{pmatrix},$$

$$\gamma = \frac{1}{3}\sqrt{(3-2k)(1+2k)(1-k^2)}.$$

Introducing the transformation $\mathbf{y} = \mathbf{T}^{-1}\mathbf{w}$,

$$\dot{\mathbf{y}} = \mathbf{J}\mathbf{y} + \frac{1}{2}\mathbf{g}^{(2)}(\mathbf{y}) + \frac{1}{6}\mathbf{g}^{(3)}(\mathbf{y}) + \mathscr{O}(\mathbf{y}^4), \tag{29}$$

where the Jordan canonical form $\mathbf{J}$ is given by

$$\mathbf{J} = \mathbf{T}^{-1}\mathscr{J}_p\mathbf{T} = \begin{pmatrix} 0 & -\omega_0 & 0 \\ \omega_0 & 0 & 0 \\ 0 & 0 & \lambda_1 \end{pmatrix}.$$

In (29), the nonlinear vector functions in transformed coordinates are given by

$$\mathbf{g}^{(2)}(\mathbf{y}) = \mathbf{T}^{-1}\mathbf{f}^{(2)}(\mathbf{w})|_{\mathbf{w}=\mathbf{T}\mathbf{y}},$$
$$\mathbf{g}^{(3)}(\mathbf{y}) = \mathbf{T}^{-1}\mathbf{f}^{(3)}(\mathbf{w})|_{\mathbf{w}=\mathbf{T}\mathbf{y}}.$$

Assuming that the center manifold has the quadratic form $y_3 = \frac{1}{2}(h_1 y_1^2 + 2h_2 y_1 y_2 + h_3 y_2^2)$, one can reduce (29) into a two-dimensional system up to third order

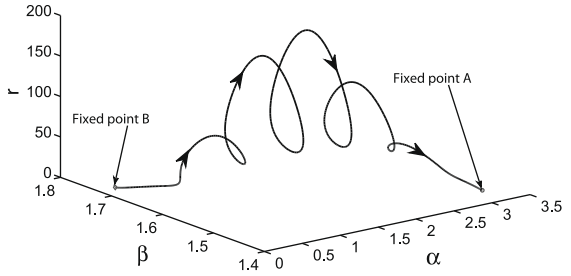

(a) Heteroclinic orbit in the phase portrait at point g

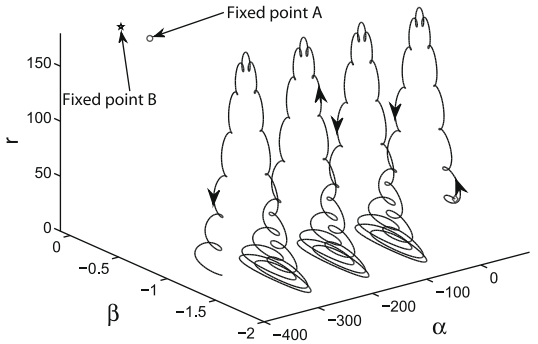

(b) Periodic orbit in the phase portrait at point g

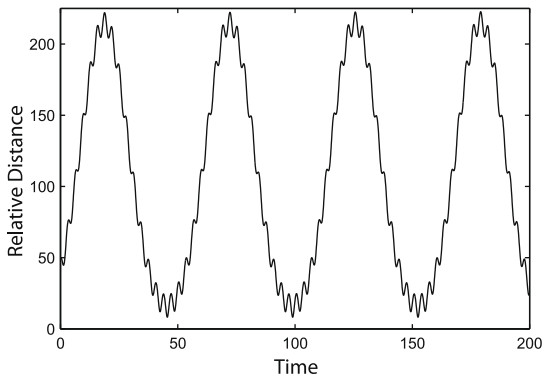

(c) Time series of the relative distance corresponding to the periodic orbit

Fig. 14. System dynamics at point *g*.

$$\begin{aligned}\dot{y}_1 &= -\omega_0 y_2 + a_{20}y_1^2 + a_{11}y_1y_2 + a_{02}y_2^2 + a_{30}y_1^3 + a_{21}y_1^2y_2 + a_{12}y_1y_2^2 + a_{03}y_2^3,\\ \dot{y}_2 &= \omega_0 y_1 + b_{20}y_1^2 + b_{11}y_1y_2 + b_{02}y_2^2 + b_{30}y_1^3 + b_{21}y_1^2y_2 + b_{12}y_1y_2^2 + b_{03}y_2^3.\end{aligned} \tag{30}$$

Using the 10 out of these 14 coefficients a_{jk}, b_{jk}, the so-called Poincaré–Lyapunov constant Δ can be calculated as [33]

$$\Delta = \frac{1}{8\omega}((a_{20}+a_{02})(a_{11}-b_{20}+b_{02}) + (b_{20}+b_{02})(a_{02}-a_{20}-b_{11})) + \frac{1}{8}(3a_{30}+a_{12}+b_{21}+3b_{03}). \tag{31}$$

Fig. 6 illustrates the variation of Δ with respect to k. Note that based on the value of parameter V, the Andronov–Hopf bifurcation can be supercritical ($\Delta > 0$) or subcritical ($\Delta < 0$).

6. Numerical results

6.1. Andronov–Hopf bifurcation

Fig. 7 shows the phase portrait corresponding to point a ($k = 0.500$, $\omega = 0.301$) on the stability chart (Fig. 5) and the associated pursuit graph. Fixed point A is exponentially attracting here. Fig. 8 depicts the phase portrait associated with point b ($k = 0.500$, $\omega = 0.408$) showing a weakly attracting fixed point A. There is a stable limit cycle born (supercritical Andronov–Hopf bifurcation) around the fixed point A (point c) when ω is increased through its critical value ω_c (phase portrait and pursuit graph are shown in Fig. 9). The pursuit trajectory in global coordinates has two harmonic components.

Fig. 10a shows the "pursuit graph" of five unicycles (initial conditions are chosen slightly away from the equilibrium formation) when ω lies slightly above the curve $\omega_2(k)$ (point c). It shows that the fourth follower exhibits most quasi-periodic behavior. The vigor of such quasi-periodicity decreases with the proximity to the leader. Fig. 10b corroborates this fact by showing that further the follower is, the wider its frequency spectrum becomes.

6.2. Fold–Hopf bifurcation

When $k > 1$, the characteristic polynomial on the stability curve $\omega_1(k)$ can be written as

$$\lambda^3 + (\omega^2 - \omega)\lambda = 0,$$

implying that there is zero eigenvalue together with a pair of pure imaginary ones. This is a Fold–Hopf (a codimension-two) bifurcation [33]. Fig. 11a and c shows the phase portrait of point f ($k = 1.20$, $\omega = 1.20$) on the stability curve $k = \omega$ and the corresponding pursuit graph, while Fig. 11b shows the phase portrait of point e situated slightly below the point f.

For the case of five unicycles (initial conditions are chosen slightly away from the equilibrium formation), the time series and the corresponding FFT for the followers are plotted in Fig. 12. It shows that the third and fourth follower exhibit complex behavior with possibly heteroclinic bursts between quasi-periodic and chaotic behavior.

6.3. Global bifurcations

In addition to the Andronov–Hopf and Fold–Hopf bifurcations, preliminary simulations indicate global bifurcations involving the destruction of heteroclinic orbits. Fig. 13 shows the phase portrait corresponding to point d ($k = 1.20$, $\omega = 0.60$), with a heteroclinic orbit connecting fixed points A and B. When k is decreased below 1, it was observed that the heteroclinic orbit disappear and the region of attraction for fixed point A shrinks significantly.

The dynamics is very interesting when k is around 1 (the intersection of the saddle-node and Andronov–Hopf bifurcation curves). When $(k, \omega) = (1.01, 1)$ (point g), one can observe a heteroclinic orbit or periodic motions containing higher harmonics as shown in Fig. 14.

7. Conclusions

In this paper, the leader–follower pursuit of unicycles is studied. Local stability analysis around the equilibrium formation has been performed. Analysis and numerical simulations have shown the existence of Andronov–Hopf and Fold–Hopf bifurcations on the stability boundary. In addition to the results provided here, the authors have also studied the effect of constant communication delay between the unicycles in leader–follower configuration. Both analytical and numerical results (not provided here) show that for a suitable distributed control law, where one may ignore the transients of the agent response, the communication has no qualitative effect on the final consensus dynamics of the agent collective. As briefly stated in Section 1, the future research direction includes the more generalized nonlinear dynamic analysis of two unicycles, not necessarily in leader–follower configuration and extending the result for multiple unicycles with communication delay.

References

[1] Parrish JK, Viscido SV, Grünbaum D. Self-organized fish schools: an examination of emergent properties. Biol Bull 2002;202:296–305.
[2] Niwa H-S. Newtonian dynamical approach to fish schooling. J Theor Biol 1996;181:47–63.
[3] Gueron S, Levin SA, Rubenstein DI. The dynamics of herds: from individuals to aggregations. J Theor Biol 1996;182:85–98.
[4] Reynolds CW. Flocks, herds and schools: a distributed behavioral model. Comput Graph 1987;21(4):25–34.
[5] McInnes CR. Distributed control for on-orbit assembly. Adv Astronaut Sci 1996;90:2079–92.
[6] Justh E, Krishnaprasad P. A simple control law for UAV formation flying. Technical Report, TR 2002-38, Institute for Systems Research, University of Maryland; 2002.
[7] Cao Y, Ren W, Sorensen N, Ballard L, Reiter A, Kennedy J. Experiments in consensus-based distributed cooperative control of multiple mobile robots. In: Proc of the 2007 IEEE international conference on mechatronics and automation; 2007. p. 2819–24.
[8] Helbing D, Farkas I, Vicsek T. Simulating dynamical features of escape panic. Nature 2000;407:487–90.
[9] Fang L, Antsaklis PJ. On communication requirements for multi-agent consensus seeking. LNCS 2006;331:53–67.
[10] Dimarogonas DV, Kyriakopoulos KJ. On the state agreement problem for unicycles. In: Proc of the 2006 American control conference; 2006. p. 2016–21.
[11] Lin J, Morse AS, Anderson BDO. The multi-agent Rendezvous problem. In: Proc of the 42nd 2003 IEEE conference on decision and control; 2003. p. 1508–13.

[12] Olfati-Saber R, Murray RM. Consensus problems in networks of agents with switching topology and time-delays. IEEE Trans Automat Contr 2004;49(9):1520–33.
[13] Bernhart A. Polygons of pursuit. Scr Math 1959;24:23–50.
[14] Marshall JA, Broucke ME, Francis BA. Formations of vehicles in cyclic pursuit. IEEE Trans Automat Contr 2004;49(11):1963–74.
[15] Marshall JA, Broucke ME, Francis BA. Pursuit formations of unicycles. Automatica 2006;42(1):3–12.
[16] Justh E, Krishnaprasad P. Steering laws and continuum models for planar formations. In: Proc of the 42nd 2003 IEEE conference on decision and control; 2003. p. 3609–14.
[17] Sepulchre R, Payley D, Leonard NE. Collective motion and oscillator synchronization. In: Kumar V, Leonard NE, Morse A, editors. Proc of the 2003 Block Island workshop on cooperative control. Berlin: Springer; 2005. p. 189–205.
[18] Klein DJ, Morgansen KA. Controlled collective motion for trajectory tracking. 2006 American control conference, Minneapolis, MN; June 2006.
[19] Desai JP, Ostrowski JP, Kumar V. Modeling and control of formations of nonholonomic mobile robots. IEEE Trans Robot Automat 2001;17(6):905–8.
[20] Das AK, Fierro R, Kumar V, Ostrowski JP, Spletzer J, Taylor CJ. A vision-based formation control framework. IEEE Trans Robot Automat 2002;18(5):813–25.
[21] Jadbabaie A, Lin J, Morse AS. Coordination of groups of mobile autonomous agents using nearest neighbor rules. IEEE Trans Automat Contr 2003;48(6):988–1001.
[22] Yang P, Freeman RA, Lynch KM. Multi-agent coordination by decentralized estimation and control. IEEE Trans Automat Contr 2008;53(11):2480–96.
[23] Freeman RA, Yang P, Lynch KM. Distributed estimation and control of swarm formation statistics. In: Proc of the 2006 American control conference, Minneapolis, MN; June 2006. p. 749–55.
[24] Lin J, Morse AS, Anderson BDO. The multi-agent rendezvous problem, Part 2: The asynchronous case. SIAM J Control Optim 2007;46(6):2120–47.
[25] Fang L, Antsaklis PJ, Tzimas A. Asynchronous consensus protocols: preliminary results, simulations and open questions. In: Proc of the 44th 2005 IEEE conference on decision and control; 2005. p. 2194–99.
[26] Liu Y, Passino KM, Polycarpou M. Stability analysis of one-dimensional asynchronous swarms. IEEE Trans Automat Contr 2003;48(10):1848–54.
[27] Gazi V. Stability of an asynchronous swarm with time-dependent communication links. IEEE Trans Syst Man Cybernet B 2008;38(1):267–74.
[28] Zhao S, Kalmár-Nagy T. Nonlinear dynamics of uni-cyclic pursuit. In: Proc of the 2008 IEEE multi-conference on systems and control, 3–5 Sep. 2008, San Antonio, TX, USA.
[29] Mathai NJ, Zourntos T. Emergent fluctuations in the trajectories of agent collectives. Fluctuat Noise Lett 2007;7(4):L429–37.
[30] Hammel D. Formation flight as an energy saving mechanism. Israel J Zool 1995;41:261–78.
[31] Andersson M, Wallander J. Kin selection and reciprocity in flight formation. Behav Ecol 2004;15(1):158–62.
[32] Levine WS. Control system fundamentals. Boca Raton (FL): CRC Press; 2000.
[33] Guckenheimer J, Holmes P. Nonlinear oscillations, dynamical systems, and bifurcations of vector fields. Berlin: Springer; 1983.
[34] Kuznetsov YA. Elements of applied bifurcation theory. Berlin: Springer; 2004.